Capillary filling under electro-osmotic effects in the presence of electromagneto-hydrodynamic effects

Nikhil Desai, Uddipta Ghosh, and Suman Chakraborty
Department of Mechanical Engineering, Indian Institute of Technology Kharagpur, West Bengal 721302, India
(Received 19 December 2013; revised manuscript received 22 April 2014; published 26 June 2014)

We report various regimes of capillary filling dynamics under electromagneto-hydrodynamic interactions, in the presence of electrical double layer effects. Our chosen configuration considers an axial electric field and transverse magnetic field acting on an electrolyte. We demonstrate that for positive interfacial potential, the movement of the capillary front resembles capillary rise in a vertical channel under the action of gravity. We also evaluate the time taken by the capillary front to reach the final equilibrium position for positive interfacial potential and show that the presence of a transverse magnetic field delays the time of travel of the liquid front, thereby sustaining the capillary motion for a longer time. Our scaling estimates reveal that the initial linear regime starts, as well as ends, much earlier in the presence of electrical and magnetic body forces, as compared to the corresponding transients observed under pure surface tension driven flow. We further obtain a long time solution for the capillary imbibition for positive interfacial potential, and derive a scaling estimate of the capillary stopping time as a function of the applied magnetic field and an intrinsic length scale delineating electromechanical influences of the electrical double layer. Our findings are likely to offer alternative strategies of controlling dynamical features of capillary imbibition, by modulating the interplay between electromagnetic interactions, electrical double layer phenomena, and hydrodynamics over interfacial scales.

DOI: 10.1103/PhysRevE.89.063017 PACS number(s): 47.61.−k

I. INTRODUCTION

Capillary filling dynamics has its applications in many diverse areas, ranging from lab-on-a-chip based micro–total analysis systems [1] to the transport of biological fluids in flora and fauna [2]. Since the pioneering contributions of Lucas and Washburn [3,4], several researchers have attempted to describe the problem of microcapillary filling in terms of a lumped (reduced-order) model [3–15], relying on an interplay between the driving surface tension forces and the resistive viscous forces, resulting in the filling length being proportional to the square root of the filling time (the so-called Washburn regime) [4–7,16–20]. Of late, researchers have probed deep into the early (inertial) regimes of capillary filling and demonstrated that there also exists a linear regime prior to the much celebrated Washburn regime, where the capillary forces and the inertial forces balance each other [5,8,9,21–26]. This results in a linear variation in the filling length with time, which has also been reported in the previous experiments conducted on capillary filling by Quere [7]. Extending the underlying considerations towards capillary filling in a vertical channel, researchers have further demonstrated that the linear regime at the initial stages of capillary filling is universal, irrespective of the orientation of the channel. Interestingly, under this scenario, the liquid front can enter either the Washburn or an oscillatory regime, depending on the strength of the viscous forces and the other opposing forces [7,9].

Despite significant advancements towards understanding the various regimes of capillary filling dynamics delineated as above, investigations on the underlying consequences under combined electromagneto-hydrodynamic effects have been relatively scarce [11]. The underlying physical issues are likely to become significantly more involved when there is a nontrivial interplay between applied electric and magnetic fields, induced electric field due to electrical double layer (EDL) formation (i.e., inception of a charged interfacial layer due to complex electrochemical interactions), and hydrodynamic effects (such as surface tension, viscous, or inertial effects) over interfacial scales [11]. Such situations, however, are omnipresent in many of the modern day lab-on-a-chip based applications in which electrical and magnetic fields may be judiciously employed to modulate the resultant capillary dynamics.

Here we investigate various regimes of capillary filling dynamics as modulated by electromagneto-hydrodynamic interactions in the presence of EDL effects. Our chosen configuration considers axial electric field and transverse magnetic field acting on an electrolyte solution. In essence, we bring out a nontrivial interplay between the external forcing parameters and interfacial phenomena over small scales towards influencing the resultant capillary dynamics. Interestingly, we delineate a gravitylike influence of the electrical interactions for interfaces with positive zeta potential. We further demonstrate that, under the action of magnetic forces, the time taken for a complete arrest of the capillary advancement is delayed, although the distance traversed remains the same, which enables one to impose critical control over sustaining the capillary motion for a larger period of time. We also demonstrate that under the present configuration, although the capillary can theoretically enter the previously reported oscillatory regime, such paradigms are practically unphysical in nature. Our scaling estimates also demonstrate that the linear regime in the capillary filling starts, as well as ends, much earlier in the presence of electrical and magnetic body forces, as compared to a simple surface tension driven capillary flow. We additionally calculate the long time solution for the capillary imbibition in cases of positive zeta potential and obtain a scaling estimate of the stopping time as a function of the strength of the magnetic field and a characteristic length scale of the EDL. Finally, we also compare our results to previously reported experiments on capillary filling [27] of charged nanochannels, in the presence of electro-hydrodynamic effects.

II. DYNAMICAL MODEL

We consider slit Hele-Shaw geometry, with the two plates being separated by a distance H. The spans of the plates in the other two directions are considered to be much larger than the height of the channel. We choose our origin at the center of the channel (see Fig. 1), with the y axis running along the transverse direction and the x axis running along the channel. A liquid front is introduced at a location $x = 0$ at time $t = 0$. The contact angle at the solid-liquid-gas (air) interface is assumed to be θ, which remains the same throughout the motion of the liquid. Additionally, an electric field is applied in the x direction, with the two electrodes placed at locations $x = 0$ and $x = L$, respectively. A constant voltage of magnitude V_0 is applied between the electrodes, which creates an axial electric field inside the channel. We further assume that the electrodes do not interfere with the motion of the fluid and the electric field is felt by the fluid only in the closed region $0 \leqslant x \leqslant L$. We also introduce a magnetic field of magnitude B_y along the transverse (y) axis, in order to assess its effects on the capillary motion of the liquid front. In addition to this, we consider the zeta potential at the shear plane of the substrate-fluid interface to be ζ. Note that this potential can bear both negative and positive values, and we will consider both cases in the present analysis. We further introduce ionic species in the liquid, with a bulk concentration of n_∞. Because of electrochemical interactions between the ionic species and the substrate, EDL forms in the vicinity of the channel walls, bearing immense consequences towards dictating the capillary dynamics.

For mathematical analysis, we consider an average position (x) of the capillary front at a time t. The equation of motion for the capillary advancement, following Newton's second law of motion, in conjunction with a reduced-order approach [12], yields

$$\frac{d}{dt}\left[(m_c + m_a)\, v\right] = F_{\text{surface}} + F_{\text{elec}} + F_{\text{mag}} + F_{\text{visc}}, \quad (1)$$

where m_c is the mass of the fluid in the capillary (per unit width) as given by $\rho H x$, v is the average velocity of the capillary (expressed as $\frac{dx}{dt}$), and m_a is the added mass (per unit width), which in the present case is represented by [12]

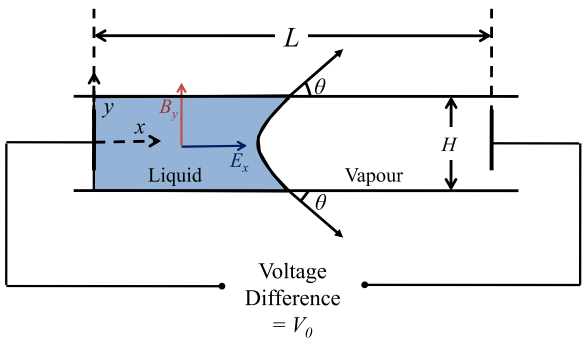

FIG. 1. (Color online) A schematic of the physical problem under consideration. A voltage difference of V_0 is applied along the x axis. A magnetic field works in the y direction. The contact angle between the wall and the liquid is θ and the surface tension is σ. The distance between the electrodes is L.

$m_a = \frac{\rho \pi H^2}{8}$, ρ being the density of the liquid. On the right-hand side of the equation, F_{surface}, F_{elec}, F_{mag}, and F_{visc} denote forces due to surface tension, electric field, magnetic field, and the viscous resistance at the walls, respectively. The surface tension force, per unit width, can be expressed as

$$F_{\text{surface}} = 2\sigma\cos\theta, \quad (2)$$

where σ is the liquid-vapor surface tension coefficient.

In an effort to estimate the electrical force in the liquid, it may be noted that the same can be expressed in terms of the product of the volumetric charge density (ρ_e) and the electric field in the liquid region [12]. The volumetric charge density, in turn, is related to the EDL potential distribution through the Poisson equation, which essentially is a differential form of the Gauss law [12]. Coupled with the Boltzmann distribution of ionic charges in the EDL, the Poisson equation essentially leads to the Poisson-Boltzmann equation, which under low surface potential limits can be suitably linearized through the Debye-Hückel approximation, to yield [12–13,28]

$$\frac{d^2\psi}{dy^2} = \kappa^2\psi. \quad (3)$$

Here, ψ is the potential within the EDL, κ is the inverse of the Debye length λ_D (characteristic length scale of the EDL) expressed as $\kappa^2 = \frac{1}{\lambda_D^2} = \frac{2z^2e^2n_\infty}{\varepsilon_l k_B T}$, z being the valency considering a z:z symmetric electrolyte, e being the protonic charge, k_B being the Boltzmann constant, T being the absolute temperature, n_∞ being the bulk concentration of electrolytes in the liquid, and ε_l being the electric permittivity of the liquid. Equation (3) can be solved with the boundary conditions $y = \pm H/2$, $\psi = \zeta$ and at $y = 0$, $\frac{d\psi}{dy} = 0$ to obtain a solution for the potential distribution as [12,29] $\psi = \zeta \frac{\cosh(\kappa y)}{\cosh(\kappa H/2)}$. Finally, one can obtain the volumetric charge density distribution as

$$\rho_e = -\varepsilon_l \frac{d^2\psi}{dy^2} = -\kappa^2\varepsilon_l\zeta \frac{\cosh(\kappa y)}{\cosh(\kappa H/2)}. \quad (4)$$

In an effort to estimate the electro-osmotic drive on the liquid in the capillary, we also need to estimate the axial potential drop across the same. Towards that, we apply our knowledge of total axial potential drop and continuity of electric displacement across the liquid-air interface and finally obtain the equations for electric fields in liquid and air as [12,14]

$$V_0 = E_l x + E_v(L - x), \quad (5a)$$

$$\varepsilon_l E_l = \varepsilon_v E_v. \quad (5b)$$

Here, the subscripts l and v denote the pertinent quantities in the liquid and the air, respectively. Equations (5a) and (5b) can be solved to obtain

$$E_l = \frac{\varepsilon_v V_0}{x\varepsilon_v + (L - x)\varepsilon_l}. \quad (6)$$

One can now evaluate the total electrical body force acting on the liquid (per unit width) from the expression [13,14]

$$F_{\text{elec}} = 2\int_0^{H/2}\int_0^x \rho_e(y)\, E_l(x) dsdy. \quad (7)$$

Using the charge distribution given in Eq. (4) and the expression for the electric field given in Eq. (6), Eq. (7) can be simplified to obtain

$$F_{\text{elec}} = \frac{-2\kappa(E_0L)\varepsilon_l\varepsilon_v\zeta.x}{\varepsilon_l L + (\varepsilon_v - \varepsilon_l)x}\tanh(\kappa H/2). \tag{8}$$

In Eq. (8), $E_0L = V_0$, where E_0 is the reference electric field, or, in other words, it is the magnitude of the electric field acting on the liquid, when the space between the electrodes is completely filled by the liquid.

The body force per unit volume of the liquid, due to the magnetic field, is given by [10,11]

$$F_{\text{body, magnetic}} = \sigma_e(\vec{E} + \vec{u} \times \vec{B}) \times \vec{B}. \tag{9}$$

Here, $\vec{u}$ is flow velocity and σ_e is the electrical conductivity of the fluid. For an applied magnetic field of magnitude B_y in the y direction, this force comes out to be $-\sigma_e B_y^2 u$ (u being the axial velocity of flow). In an effort to estimate the flow velocity, we consider a fully developed flow profile generated by means of application of external axial electric ($E_x\mathbf{e_x}$) and transverse magnetic fields ($B_y\mathbf{e_y}$) along with a pressure gradient, which originates from the capillary forces. The Navier-Stokes equation then reads [10]

$$-\frac{dp}{dx} + \eta\frac{d^2u}{dy^2} - \sigma_e B^2 u - \kappa^2\varepsilon E_l\zeta\frac{\cosh(\kappa y)}{\cosh(\kappa H/2)} = 0, \tag{10}$$

where μ is the viscosity of the liquid. Note that in Eq. (10), E_l is the axial electric field acting on the liquid phase and σ_e is the electrical conductivity of the liquid. The solution of (10) nondimensionalized with the Helmholtz-Smoluchowski velocity, subject to no-slip boundary conditions at the walls, reads

$$\bar{u} = \frac{u}{u_{\text{HS}}} = -\frac{\bar{\kappa}^2}{\bar{\kappa}^2 - \text{Ha}^2}\left\{\frac{\cosh(\bar{\kappa}\,\bar{y})}{\cosh(\bar{\kappa}/2)} - \frac{\cosh(\text{Ha}\bar{y})}{\cosh(\text{Ha}/2)}\right\} - \frac{P}{\text{Ha}^2}\left\{1 - \frac{\cosh(\text{Ha}\bar{y})}{\cosh(\text{Ha}/2)}\right\}. \tag{11}$$

In Eq. (12), Ha is the Hartmann number [10], given by $\text{Ha} = \frac{\sigma_e B_y^2}{\mu/H^2}$, $\bar{y} = y/H$; $P = \frac{H^2(dp/dx)}{\eta u_{\text{HS}}}$, $u_{\text{HS}} = \frac{-\varepsilon_l E_l\zeta}{\mu}$ is the Helmholtz-Smoluchowski velocity and $\bar{\kappa} = \kappa H$. From (11) one can easily find the average velocity, which reads

$$\bar{u}_{\text{avg}} = \frac{u_{\text{avg}}}{u_{\text{HS}}} = -\frac{\bar{\kappa}^2}{\bar{\kappa}^2 - \text{Ha}^2}\left\{\frac{\tanh(\bar{\kappa}/2)}{(\bar{\kappa}/2)} - \frac{\tanh(\text{Ha}/2)}{(\text{Ha}/2)}\right\} - \frac{P}{\text{Ha}^2}\left\{1 - \frac{\tanh(\text{Ha}/2)}{(\text{Ha}/2)}\right\}. \tag{12}$$

Therefore, following (11), the velocity can be expressed in terms of the average velocity in the following way:

$$u = \frac{(dx/dt)}{\bar{u}_{\text{avg}}}\left[-\frac{\bar{\kappa}^2}{\bar{\kappa}^2 - \text{Ha}^2}\left\{\frac{\cosh(\bar{\kappa}\,\bar{y})}{\cosh(\bar{\kappa}/2)} - \frac{\cosh(\text{Ha}\bar{y})}{\cosh(\text{Ha}/2)}\right\} - \frac{P}{\text{Ha}^2}\left\{1 - \frac{\cosh(\text{Ha}\bar{y})}{\cosh(\text{Ha}/2)}\right\}\right]. \tag{13}$$

In (13) we have replaced, u_{avg} with dx/dt, i.e., the velocity of the liquid front. We can now evaluate the viscous resistance using the expression [30]

$$F_{\text{visc}} = 2x\tau_w = 2x\mu\left.\frac{du}{dy}\right|_{y=-H/2}. \tag{14}$$

Using (13) in (14), we can express the total viscous resistance to the flow in the following way:

$$F_{\text{visc}} = \frac{-2\mu x(dx/dt)}{H}\frac{(\bar{F}_1 + G\bar{F}_2)}{(K_1 + GK_2)}. \tag{15}$$

In Eq. (15), the various symbols represent

$$\bar{F}_1 = \tanh(\text{Ha}/2)/\text{Ha},$$

$$\bar{F}_2 = -\frac{\bar{\kappa}^2}{\bar{\kappa}^2 - \text{Ha}^2}\{\text{Ha}\tanh(\text{Ha}/2) - \bar{\kappa}\tanh(\bar{\kappa}/2)\}$$

$$K_1 = \frac{1}{\text{Ha}^2}\left\{1 - \frac{\tanh(\text{Ha}/2)}{(\text{Ha}/2)}\right\},$$

$$K_2 = -\frac{\bar{\kappa}^2}{\bar{\kappa}^2 - \text{Ha}^2}\left\{\frac{\tanh(\bar{\kappa}/2)}{(\bar{\kappa}/2)} - \frac{\tanh(\text{Ha}/2)}{(\text{Ha}/2)}\right\},$$

and

$$G = 1/P = \frac{\eta u_{\text{HS}}}{H^2(dp/dx)} = \frac{-\varepsilon_l E_0\zeta}{H^2(dp/dx)}.$$

Therefore, the contribution of the pressure gradient in the viscous resistance comes in the analysis, through the constants $\bar{F}_1$ and K_1 as evident from Eq. (15). It is important here to investigate typical orders of magnitude of the pressure gradient (dp/dx). As mentioned earlier, this pressure gradient is mainly caused by the surface tension force (i.e., the Laplace pressure). Now, the pressure drop across the liquid-air interface is $\Delta p = \sigma/R$, where R is the radius of curvature and in the present case $R = H/(2\cos(\theta))$. This drop in pressure occurs over a distance of x, i.e., the length of the liquid column. Therefore, the pressure gradient can be taken as $-\frac{dp}{dx} = \frac{\sigma}{Rx}$ in Eq. (15).

Next, we can express the total force acting on the liquid due to the application of the magnetic field with the help of Eq. (9), and the magnetic body force (per unit width) finally takes the form

$$F_{\text{mag}} = -2\int_{x=0}^{x=x}\int_{y=0}^{y=H/2}\sigma_e B_y^2 u\,ds\,dy. \tag{16}$$

Using expression (13) for the velocity field and assuming σ_e to remain constant throughout the cross section, we obtain F_{mag} to be

$$F_{\text{mag}} = -\frac{\mu}{H}\text{Ha}^2 x\frac{dx}{dt}, \tag{17}$$

where $\frac{dx}{dt} = u_{\text{avg}}$ denotes the average rate of capillary displacement [3–15]. Thus the equation for capillary filling can be finally expressed as [substituting (2), (8), (15), and (17) in (1)]

$$\frac{d}{dt}\left[\left(\rho Hx + \frac{\rho\pi H^2}{8}\right)\frac{dx}{dt}\right] = 2\sigma\cos\theta - \frac{2\kappa(E_0L)\varepsilon_l\varepsilon_v\zeta.x}{\varepsilon_l L + (\varepsilon_v - \varepsilon_l)x}\tanh(\kappa H/2) - \frac{\mu}{H}\text{Ha}^2 x\frac{dx}{dt} - \frac{2\mu x(dx/dt)}{H}\frac{(\bar{F}_1 + G\bar{F}_2)}{(K_1 + GK_2)}. \tag{18}$$

Note that in (18), G is given by $G = \frac{-\varepsilon_l E_0 \zeta}{H^2(dp/dx)}$. Equation (18) represents a general description of the capillary filling process. The advantage of including the pressure gradient in the description of the viscous forces has been clearly delineated later in Sec. V. Having derived a general (lumped) description of capillary filling process, we now attempt to do a simple scaling analysis, in an effort to deduce the contribution of the pressure gradient term in the viscous force.

Towards this we note that, by virtue of the linearity of Eq. (10) one can divide the viscous stress into two parts, τ_p and τ_e, where the subscript "p" denotes the contribution of the pressure gradient and "e" denotes the contribution of the electro-osmotic part. One can write the viscous stress due to pressure as $\tau_p \sim \mu u_p/H$, where $u_p \sim H^2(dp/dx)/\mu$. Therefore, the stress becomes $\tau_p \sim H(dp/dx) \sim \sigma/x$. On the other hand, the velocity profile due to electro-osmotic flow alone is $u_e = -\frac{\varepsilon_l \zeta E_0}{\eta}(1 - \frac{\psi}{\zeta})$ (symbols bear the usual meanings). In the case of electro-osmotic flows the velocity develops from zero value at the wall to a near constant value within the Debye layer, i.e., within a length of $O(\kappa^{-1})$ of the wall (κ is the inverse of the characteristic EDL thickness). Therefore, the viscous stress for electro-osmotic flow is on the order of $\tau_e \sim \varepsilon_l E_0 \zeta \kappa$. Hence it follows that the ratio of the two stress components is given by $r \sim \tau_p/\tau_e \sim \frac{\varepsilon_l E_0 \zeta \kappa x}{\sigma} = G\kappa \sim G\bar{F}_2$ [note that $\bar{F}_2 \sim \bar{\kappa}$ in (15)]. For the present analysis we have chosen the following values of the required parameters: $H \sim 10^{-4}$ m, $\mu \sim 10^{-3}$ Pa s, $\varepsilon_l \sim 6 \times 10^{10}$ F/m, $\zeta \sim 0.05$ V, $E_0 \sim 10^6$ V/m, and $\kappa \sim 10^7$–10^8 m^{-1} along with $x \sim J \sim 0.1$ m (J is the equilibrium position, or modified Jurin height). Putting these values in the aforementioned ratio ($r \sim G$), we get $G\kappa \sim Ax$, where $A \sim O(10^3$–$10^4)$. Therefore, with x in centimeters ($x \sim 0.1$), $G\kappa \sim O(10^2$–$10^3)$. This scaling basically indicates that the order of magnitude of the contribution of viscous stresses from electro-osmotic flows outweighs the same due to the pressure gradient driven flow component. It is quite simple to show that (with a similar analysis), if the viscous stress from pressure driven flow is to be as important as those due to electro-osmotic flow, we must have for the present case $dp/dx \sim O(10^7)$ Pa/m, which is quite large as compared to the Laplace pressure gradient on the capillary.

Following the previous scaling analysis, we simplify Eq. (15), when the capillary filling is assisted by external applied electric field and only take into account the viscous forces originating from the electro-osmotic flows. Towards this, we neglect the terms $\bar{F}_1$ and K_1 and write (15) as (i.e., we neglect the effect of pressure gradient on viscous resistance as well as the average velocity)

$$F_{\text{visc}} = \frac{-2\mu x(dx/dt)}{H}\frac{\bar{F}_2}{K_2}. \tag{19}$$

Using (18) in (19) we get

$$\frac{d}{dt}\left[\left(\rho H x + \frac{\rho\pi H^2}{8}\right)\frac{dx}{dt}\right] = 2\sigma\cos\theta - \frac{2\kappa(E_0 L)\varepsilon_l\varepsilon_v\zeta.x}{\varepsilon_l L + (\varepsilon_v - \varepsilon_l)x}\tanh(\kappa H/2) - \frac{\mu}{H}\text{Ha}^2 x\frac{dx}{dt} - \frac{2\mu x(dx/dt)}{H}\frac{\bar{F}_2}{K_2}. \tag{20}$$

From here onwards, all our results (except those in Sec. V B) have been obtained solving Eq. (20). It is important to mention that a similar approach has previously been adopted by a number of researchers [12,14] for analyzing capillary filling in the presence of electrical effects. Equation (20) can be nondimensionalized using the following reference values $\bar{x} = \frac{x}{L}$, $\bar{t} = \frac{t}{t_0}$, where $t_0 = \sqrt{\frac{\rho H L^2}{2\sigma}}$ (which has been calculated from balancing the inertial and the capillary force terms). The nondimensionalized equation is given by

$$\frac{d}{d\bar{t}}\left[\left(\bar{x} + \frac{\pi H}{8L}\right)\frac{d\bar{x}}{d\bar{t}}\right] = \cos\theta - \frac{E_0 L\varepsilon_l\zeta}{\sigma H}\bar{x}\bar{E}\bar{\kappa}\tanh(\bar{\kappa}/2) - \frac{\mu L\text{Ha}^2}{H\sqrt{2\sigma\rho H}}\bar{x}\frac{d\bar{x}}{d\bar{t}} - \frac{\eta L}{\sqrt{2\sigma\rho H}}\bar{x}\frac{d\bar{x}}{d\bar{t}}. \tag{21}$$

Note that in Eq. (21), $\bar{E} = \frac{1}{\bar{x}+(1-\bar{x})\bar{\varepsilon}}$, $\bar{\varepsilon} = \frac{\varepsilon_l}{\varepsilon_v}$, and η is given by

$$\eta = \frac{2\mu}{H}\frac{[-\bar{\kappa}\sinh(\bar{\kappa}/2) + \text{Ha}\cosh(\bar{\kappa}/2)\tanh(\text{Ha}/2)]}{\left[\frac{\sinh(\bar{\kappa}/2)}{\bar{\kappa}/2} - \frac{\cosh(\bar{\kappa}/2)\tanh(\text{Ha}/2)}{\text{Ha}/2}\right]}.$$

There are several interesting points to note from Eq. (21). The first one is that the sign of the second term on the right-hand side, i.e., the electrical body force, depends on the sign of the zeta potential, which indicates that in cases of positive zeta potential, the capillary motion is opposed by the electric field and in cases of negative zeta potential, the capillary motion is aided by the electric field. This naturally indicates that the capillary motion for positive zeta potential is likely to mimic the dynamics of the same under the action of gravity. Therefore, the capillary is likely to stop after traversing a certain distance, which can be inferred to be dictated by several relevant parameters such as the strength of the electric field, the EDL thickness, etc. We elaborate more on this in the next section. Secondly, it should be noted from Eq. (21) that the magnetic force actually opposes the motion of the capillary. Quite interestingly, it has the same form as that of the viscous resistance force, which indicates that the magnetic force acts as an effective magneto-viscous resistance against the motion of the capillary. Another important point to note here is that, for $\bar{x} = 1$, i.e., when the capillary front fills the whole space between the two electrodes, the electric field takes a value $\bar{E} = 1$ and remains constant at that value as the capillary progresses further. This indicates that, after the capillary crosses the location $\bar{x} = 1$, the electrical body force, acting on the liquid becomes constant, expressed as $\bar{F}_{\text{elec}} = -\frac{E_0 L\varepsilon_l\zeta}{\sigma H}\bar{\kappa}\tanh(\bar{\kappa}/2)$.We elaborate further on these individual forces along with the motion of the capillary, when we present the detailed solution for the position of the capillary front as a function of time.

Equation (21) is not analytically tractable, though several approximate solutions can be determined based on various simplifying assumptions, the most notable among them being the short and the long time solutions for the capillary motion. We represent scaling estimates for the early filling regimes, derive long time solutions and scaling estimates of the stopping

time (for positive zeta potential), and compare those with the corresponding numerical solutions in the subsequent section.

III. SCALING ESTIMATES

In this section, we execute an order of magnitude analysis for various forces at play and attempt to derive a simple scaling relation between the filling length and the time of filling. First, we will attempt to reveal the important forces, dictating the capillary motion during early times of filling. Later in this section, we derive a long time solution for the capillary motion in cases of positive zeta potential (i.e., when the electrical body force is opposing the motion of the capillary) and present a scaling estimate for the time required for the capillary to stop. In the subsequent sections, we attempt to compare our scaling estimates and the approximate solutions with the full numerical solutions to Eq. (21).

A. Early transients of capillary filling

1. Inviscid regime

It has been previously demonstrated by Das *et al.* [8] that at the beginning of the filling process, the viscous and other body forces are negligible, which indicates that a balance between the inertial forces (F_{inertia}) and the capillary forces ($F_{\text{s.t.}}$) should be maintained during the motion. This is mathematically justified by virtue of the fact that the filling length is too small for the body and viscous forces, which are proportional to the filling length, to have any significant contribution. Thus

$$F_{\text{inertia}} \sim F_{\text{surface}}. \tag{22a}$$

When the respective forces are expressed per unit width, $F_{\text{inertia}} \sim \frac{d}{dt}(\rho H x \frac{dx}{dt}) \sim \frac{\rho H x^2}{t^2}$ (where x is the filling length) and $F_{\text{surface}} \sim \sigma$, so that

$$\frac{\rho H x^2}{t^2} \sim \sigma \Rightarrow x \sim t\sqrt{\frac{\sigma}{\rho H}}. \tag{22b}$$

Note that the expression in (22b) remains independent of other body forces and surface forces, characterizing early regimes of capillary filling [9]. However, we must acknowledge that the ranges of x and t, over which Eq. (22b) remains valid, cannot be ascertained from the above considerations alone.

2. Washburn regime

As the capillary progresses along the channel, the viscous forces gradually increase in magnitude and start to dominate. The viscous force (per unit width) can be scaled as $F_{\text{visc}} \sim \mu \frac{\partial u}{\partial y} x$. Since the velocity profile in the capillary is considered to be dictated largely by the electrokinetic effects (the electrokinetic effects are designed to be the primary flow actuation mechanisms considered in this work), the viscous force comes out to be on the order of $F_{\text{visc}} \sim \mu u \kappa x$. Note that here $\kappa = 1/\lambda_D$ is the inverse of the Debye length, which in turn is the characteristic length scale of the EDL formed. This estimation is based on the fact that for electro-osmotic flow (EOF), the velocity attains its highest magnitude at the edge of the EDL, thus making the shear rate near the wall to be of the order of $\sim u\kappa$. Note that additionally there is a magnetic force, which basically acts as an equivalent viscous resistance and is proportional to the Hartmann number squared (Ha^2). However, we also note that in the channel considered in the present study, $\kappa \gg 1$, whereas $\text{Ha} \sim 1$ at best. Therefore, for the scaling of viscous forces, it is sufficient to consider $F_{\text{visc}} \sim \mu u \kappa x$. In the Washburn regime, the balance is between the viscous force and the forward pulling capillary force, which gives us

$$F_{\text{visc}} \sim F_{\text{s.t}} \Rightarrow \mu u \kappa x \sim \sigma. \tag{23a}$$

Again, noting that $u \sim x/t$, we finally have

$$x \sim \sqrt{t}\sqrt{\frac{\sigma}{\mu\kappa}}. \tag{23b}$$

The above expression essentially delineates the capillary transport characteristics over the Washburn regime, subjected to electrokinetic effects.

Next, we attempt to answer the question: What is the temporal instance characterizing the initiation of the Washburn regime? This is essentially determined by the ratio of the viscous force and the forward pulling surface tension forces [8,9], which can be expressed as $\frac{F_{\text{visc}}}{F_{\text{s.t}}} \sim \frac{\mu\kappa x^2/t}{\sigma}$. Noting that in the linear regime $\frac{x}{t} \sim \sqrt{\sigma/\rho H}$, we get

$$\frac{F_{\text{visc}}}{F_{\text{s.t}}} \sim \frac{\mu\kappa x^2/t}{\sigma} \sim \frac{\mu}{\sqrt{\rho H \sigma}} \frac{x}{H} \bar{\kappa} \sim \text{Oh}\left(\frac{x}{H}\right)\bar{\kappa}. \tag{24}$$

In Eq. (24), Oh is the Ohnesorge number defined as $Oh = \mu/\sqrt{\rho H \sigma}$. Since in the linear regime viscous forces are small, it follows that for relation (22b) to hold true, we must have [8]

$$\frac{F_{\text{visc}}}{F_{\text{s.t}}} \ll 1 \Rightarrow \text{Oh}\left(\frac{x}{H}\right)\bar{\kappa} \ll 1. \tag{25}$$

Now, for water, $\mu \sim 1$ mPa s, $\sigma \sim 0.07$ N/m (air water interface), and $\rho \sim 10^3$ kg/m^3. For a channel height of $H \sim 500$ μm (we typically consider micrometer dimensions or less so that EDL effects may turn out to be important as compared to other volumetric effects), we get $\text{Oh} \sim 0.005$. However, the EDL thickness is, at maximum, of the order of $\kappa^{-1} \sim 100$ nm, for salt concentration of the order of 0.1 mM, which makes $\bar{\kappa} \sim 100 - 1000$. Hence, $\text{Oh}\bar{\kappa} \sim 0.5$–$5$. This indicates that for condition (25) to hold in this particular case, we must also have $x \ll H$ in addition to the very low value of Oh. Here, it is noteworthy that for capillary filling without electromagneto-hydrodynamic interactions [8], the Washburn regime starts when $\text{Oh}(\frac{x}{H}) \sim 1$. On the contrary, the equivalent condition here is $\text{Oh}(\frac{x}{H}) \sim 1/\bar{\kappa}$, which simply indicates that for electrically driven capillary motion, the Washburn regime sets in very early (since $\bar{\kappa} \gg 1$, for the channel dimensions considered in the present study). The above scaling analysis further indicates that the linear regime persists for a value of $x \ll H$. This is in sharp contrast to the classical capillary filling [8], where we have the linear regime prevailing even for x as high as $\sim H$. This shift of paradigm is because of the influence of the electro-osmotic velocity profile towards dictating the viscous resistances.

B. Long time solution

We first attempt to estimate the equilibrium length achieved by the capillary (equivalent to "Jurin" height [7]) under the action of electrical forces. This can be simply achieved by

balancing the capillary forces and the electrical body force, expressed in Eqs. (2) and (8). This equilibrium length takes the form

$$\bar{L}_s = \frac{\bar{\varepsilon}}{\frac{E_0 L \varepsilon_l \zeta}{\sigma H}\frac{\bar{\kappa}\tanh(\bar{\kappa}/2)}{\cos\theta} + \bar{\varepsilon} - 1}. \tag{26}$$

Here, $\bar{L}_s$ is the position of the capillary front, when the said forces equilibrate and the front stops advancing. One interesting point to note from the expression (26) is that the equilibrium position does not depend on the Hartmann number, or equivalently, the strength of the applied magnetic field. This is understandable, since the magnetic field only exerts a net force on the liquid, when it is moving and hence, the equilibrium position, where the capillary stops moving, is not affected by the presence of the magnetic field. Higher values of θ and κ shorten the equilibrium position, as attributable to less forward pulling surface tension force and higher opposing electrical force, respectively. However, it is important to note that in deriving Eq. (26), we have used the relation (6), which only remains valid until $\bar{x} \leqslant 1$ ($\bar{x}$ is the capillary position). This indicates that $\bar{L}_s$ must satisfy the relation $\bar{L}_s \leqslant 1$ in order for Eq. (26) to be valid, which suggests that the capillary will always stop between the two electrodes, if it stops at all. Once the capillary crosses the far side electrode, positioned at $\bar{x} = 1$, the opposing electrical force becomes constant, as mentioned in the previous section, which finally results in an unarrested motion of the capillary.

Having derived the equivalent "Jurin" height or the equilibrium length for the liquid, we now attempt to derive a long time approximate solution of the governing equation (21), in an effort to highlight the behavior of the capillary, when it is close to the "Jurin length." In such cases, we can assume $\Delta\bar{x} = \bar{L}_s - \bar{x} \ll 1$, again following Lucas [3] and Washburn [4]. Recasting Eq. (21) in terms of $\Delta\bar{x}$, we can write

$$0 = A - \frac{B(\bar{L}_s - \Delta\bar{x})}{a}\left[1 - \frac{\Delta\bar{x}(\bar{\varepsilon}-1)}{a} + O(\Delta\bar{x}^2)\right] + (C+D)\bar{L}_s\frac{d\Delta\bar{x}}{d\bar{t}}. \tag{27}$$

In Eq. (27), the constants are given by $A = \cos\theta$, $B = \frac{E_0 L \varepsilon_l \zeta \bar{\kappa}\tanh(\bar{\kappa}/2)}{\sigma H}$, $C = \frac{\mu L \mathrm{Ha}^2}{H\sqrt{2\sigma\rho H}}$, and $D = \frac{\eta L}{\sqrt{2\sigma\rho H}}$. In deriving Eq. (27), we have neglected the inertial forces. This is justified in that just before the equilibrium height is achieved, the front velocity becomes negligibly small and so does the inertia of the liquid column. Additionally, this equation overestimates the resistive forces as it assumes the wetted area to remain constant as evident from the last term in the equation. However, the opposing electrical force is underestimated, since it is represented in a linearized form as a function of $\Delta\bar{x}$. Equation (27) can be solved for $\Delta\bar{x}$, with the initial conditions at $\bar{t} = 0$, $\Delta\bar{x} = \bar{L}_s$ to obtain a solution of the type

$$\Delta\bar{x} = \bar{L}_s \exp\left[\frac{-k\bar{t}}{(C+D)\bar{L}_s}\right]. \tag{28}$$

Here, $k = \frac{B\bar{\varepsilon}}{a^2}$ and $a = \bar{L}_s + \varepsilon(1 - \bar{L}_s)$. Finally, using Eq. (28), one can obtain an expression for $\bar{x}$ of the form

$$\bar{x} = \bar{L}_s\left\{1 - \exp\left[\frac{-k\bar{t}}{(C+D)\bar{L}_s}\right]\right\}. \tag{29}$$

This analysis predicts an exponential variation in the capillary rise, when it is close to the equilibrium length. Additionally, we can also obtain an approximate estimation for the time taken by the capillary to reach the equilibrium position, which in the present case turns out to be $\bar{t}_s \sim O[\frac{(C+D)\bar{L}_s}{k}]$. It essentially indicates that the presence of the magnetic field delays the time taken by the capillary to reach the equilibrium position, or, in other words, the motion of the capillary is sustained for a longer time when a transverse magnetic field is applied. We note that, for small Hartmann numbers, i.e., for $\mathrm{Ha} \ll 1$, $\eta \sim \frac{\mu\bar{\kappa}}{H}$, assuming that $\bar{\kappa} \gg 1$. Hence, $C \sim \frac{\mu L \mathrm{Ha}^2}{H\sqrt{\sigma\rho H}}$ and $D = \frac{\eta L}{\sqrt{2\sigma\rho H}} \sim \frac{\mu\bar{\kappa}L}{H\sqrt{\sigma\rho H}}$, again for $\bar{\kappa} >> 1$. Therefore, $C + D \sim \frac{\mu L}{H\sqrt{\sigma\rho H}}(\bar{\kappa} + \mathrm{Ha}^2) \sim \frac{\mu\bar{\kappa}L}{H\sqrt{\sigma\rho H}}$, since $\bar{\kappa} \gg 1$ and $\mathrm{Ha} \ll 1$. Noting that $k = \frac{B\bar{\varepsilon}}{a^2}$ (for $\bar{\kappa} \gg 1$), we finally can have a scaling estimate for the filling time, which takes the form

$$\bar{t}_s \sim \frac{\bar{L}_s a^2}{B\bar{\kappa}\bar{\varepsilon}}\frac{\mu\bar{\kappa}L}{H\sqrt{\sigma\rho H}}. \tag{30}$$

Contrary to Eq. (30), for $\mathrm{Ha} \gg 1$, we get $\eta \sim \frac{\mu\bar{\kappa}\mathrm{Ha}}{H}$ and $C + D \sim \frac{\mu L}{H\sqrt{\sigma\rho H}}(\bar{\kappa}\mathrm{Ha} + \mathrm{Ha}^2)$. This simply indicates that the filling time takes the form

$$\bar{t}_s \sim \frac{\bar{L}_s a^2}{B\bar{\kappa}\bar{\varepsilon}}\frac{L\mu}{H\sqrt{\sigma\rho H}}(\mathrm{Ha}^2 + \bar{\kappa}\mathrm{Ha}). \tag{31}$$

We conclude from estimates (30) and (31) that for low values of Hartmann numbers the filling time is virtually independent of the magnetic field strength, whereas for higher values of the same, the filling time roughly varies quadratically with Ha. The whole analysis has been executed using $\bar{\kappa} \gg 1$. This is well justified, since the EDL thickness at best is ~100 nm and hence $\kappa \sim 10^7$. For a channel height $H \sim 100$ μm, $\bar{\kappa} \sim 100 - 1000 \gg 1$.

IV. RESULTS AND DISCUSSIONS

A. Comparison of scaling estimates and actual numerical solutions

We next attempt to compare the scaling analysis executed in the previous section with the full scale numerical solutions of Eq. (21). Towards this, we first compare the scaling estimates for the early linear regime as reported in Sec. III A, with the numerical solution. It is important to mention here that we have taken the electrode spacing to be 10 cm and the applied voltage difference between the two electrodes to be 10^5 V [12], throughout the analysis. Figure 2 depicts the comparative results of scaling for initial capillary filling dynamics as given in Eqs. (22b) and (23b) (i.e., the linear and the Washburn regimes) and the numerical solution to Eq. (21), while the relevant parameters have been mentioned in the figure caption. A good agreement can be observed between the numerical and the scaling estimates. Note that the scaling estimates have been plotted in the form $x_{\mathrm{inviscid}} = M_1 t\sqrt{\frac{\sigma}{\rho H}}$ and $x_{\mathrm{Washburn}} = M_2\sqrt{t}\sqrt{\frac{\sigma}{\mu\kappa}}$, where M_1 and M_2 are constants with values 1.0204 and 1.1769. As mentioned in Sec. III A 1, the linear regime lasts for a very short time at the beginning, where x (filling length) varies roughly as 10^{-6}–10^{-4} m. This implies that the majority of the linear regime persists over a

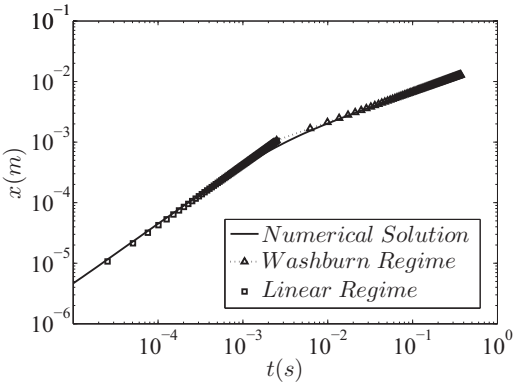

FIG. 2. Comparison between the scaling estimates and numerical solutions. We have plotted the linear regime (squares) represented in Eq. (22b), and the modified Washburn regime (dotted line, with triangles) in Eq. (23b) along with the full solution of Eq. (20) (continuous black line). The other relevant parameters have been taken as $\bar{\kappa} = 100$, Ha $= 1$, $\theta = 45°$, $\zeta = 50$ mV. The x axis (time, t) is in seconds (s) and the y axis (displacement, x) is in meters (m).

span much shorter than the channel height (for example, $H = 500\ \mu$m, as considered throughout the present section). This linear regime lasts until a time scale of $t \sim 1$ ms. Therefore, a simple comparison of the present figure with the scaling estimate previously derived by Das *et al.* [8] clearly reveals that the linear regime in the present case has a much shorter span than that realized in gravity-influenced capillary filling. We also depict the Washburn regime in the same figure, where the surface tension is balanced by viscous forces. This regime starts much earlier (around $x \sim 0.1$ mm and $t \sim 1$ ms) as compared to simple surface tension assisted capillary filling demonstrated by Das *et al.* [8].

Figure 3 depicts the comparison between the approximate long time solution and the full numerical solution of Eq. (20), the other relevant parameters being mentioned in the caption. We observe that these two solutions start matching from $\bar{t} \sim 200$, whereas at earlier times the present solution overestimates the location of the capillary as the higher-order terms neglected in the expression for the electric field in Eq. (27) become important.

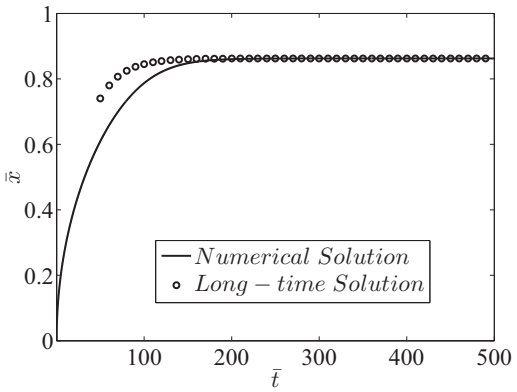

FIG. 3. Comparison between the long time approximate solution of Eq. (27) (black circles) and full numerical solution of Eq. (20) (continuous black line). The other relevant parameters are given by $\zeta = 50$ mV, $\bar{\kappa} = 100$, $\theta = 45°$, and Ha $= 1$.

B. General solution and stopping time

Having compared the scaling estimates and the numerical solutions for capillary filling, we now attempt to present the general solutions of filling distance as functions of time, obtained from Eq. (21).

1. Implications of positive zeta potential

It has been pointed out earlier that for positive surface potential on the walls, the capillary might stop after traversing a certain distance, depending on the strength of the applied electric field and other relevant parameters such as the magnitude of the interfacial potential, characteristic EDL thickness, etc. In this respect, it has also been mentioned that the electrical forces can be used to oppose the motion, much in the same manner as gravity, to arrest the capillary advancement. However, the present method gives us more precise control over the motion of the capillary, since we can tune the strength of the electric field and also modify the other relevant parameters.

In Fig. 4(a), we plot the capillary position ($\bar{x}$) as a function of time, for different Hartmann number values. The figure shows that the capillary stops at a position $\bar{x} \sim 0.9$, where, as

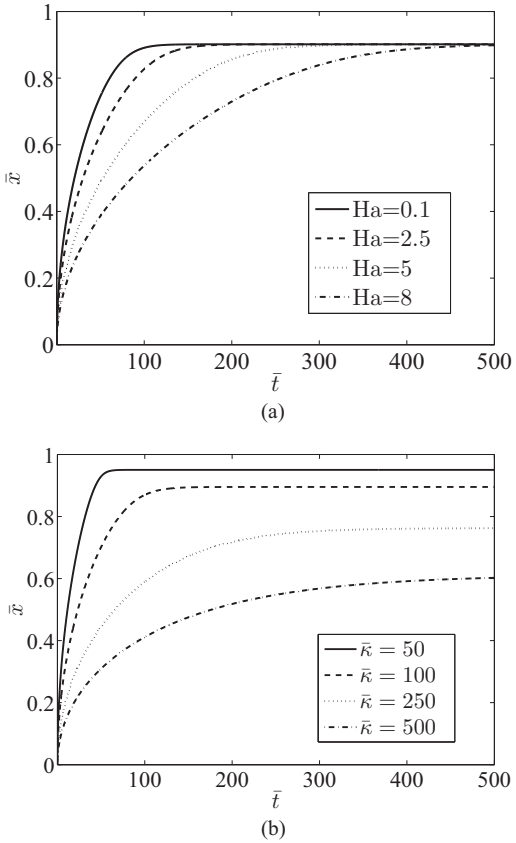

FIG. 4. (a) $\bar{x}$ vs $\bar{t}$, for $\zeta_0 = 50$ mV, $\bar{\kappa} = 100$, and $\theta = 0°$, with varying Hartmann numbers given by: Ha $= 0.1$, 2.5, 5, and 8. (b) $\bar{x}$ vs $\bar{t}$ with Ha $= 1$, $\zeta_0 = 50$ mV, and $\theta = 20°$, for different values of $\bar{\kappa} = 50$, 100, 250, and 500.

explained earlier, the surface tension force and the body force due to electric field balance each other. While deriving the long term solution in Eq. (29), we demonstrated that the capillary filling time increases due to the presence of the magnetic field. The figure indeed shows that the capillary takes more time to reach the final equilibrium position, when Ha is increased. Again, we observe that the equilibrium position is not altered by the magnetic field, which is in accordance with Eq. (26). The trend of a delay in the filling can be explained from the fact that the effect of the magnetic field essentially acts as an equivalent magneto-viscous force, which opposes the motion of the capillary, as evident in Eq. (21). Therefore, an increase in Ha slows down the capillary, which takes more time to reach the final equilibrium position.

Figure 4(b) depicts the position of the capillary as a function of time, for different values of characteristic EDL thickness, the inverse of which is denoted by $\bar{\kappa}$. Again the capillary finally reaches an equilibrium position, but now this equilibrium length decreases as we increase the value of $\bar{\kappa}$, which is in accordance with Eq. (26). We further observe that the time taken by the capillary to reach the final position also increases with $\bar{\kappa}$, which can be attributed to the fact that, as we increase $\bar{\kappa}$, the opposing body force due to the axial electric field increases, along with the viscous resistance as expressed in Eq. (19). As a consequence, the equilibrium length drops and the capillary is slowed down, which leads to an increase in the time of movement.

In Fig. 5, we demonstrate the variation in the time taken ($\bar{t}_s$) by the capillary to reach the final equilibrium position with Ha, while the other relevant parameters have been mentioned in the caption. Along with the time obtained from the numerical solutions, we also plot the scaling estimates for the stopping time, presented in Eqs. (30) and (31). The scaling estimates are plotted in the form $\bar{t}_s = M_3 \frac{\bar{L}_s a^2}{B\bar{\kappa}\varepsilon} \frac{\mu\bar{\kappa}L}{H\sqrt{\sigma\rho H}}$ for Ha $\ll 1$ and $\bar{t}_s = M_4 \frac{\bar{L}_s a^2}{B\bar{\kappa}\varepsilon} \frac{L\mu}{H\sqrt{\sigma\rho H}}(\mathrm{Ha}^2 + \bar{\kappa}\mathrm{Ha})$ for Ha $\gg 1$, where M_3 and M_4 are constants, with values 5.4650 and 5.2126, respectively. Quite

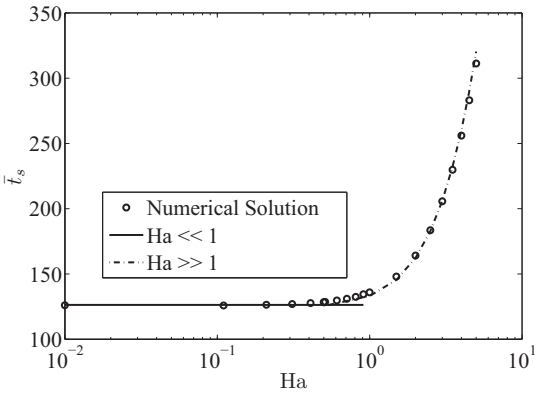

FIG. 5. Comparison of scaling estimates of the capillary filling time (t_s) with the numerically estimated time from the solution of Eq. (20). The scaling estimate for the small Ha [Eq. (30)] is represented by the continuous black line and the same for large Hartmann numbers [Eq. (31)] is denoted by dot-dash line. Black circles denote the numerical estimate of t_s. Other relevant parameters are $\bar{\kappa} = 100$, $\theta = 45$, $\zeta = 50$ mV.

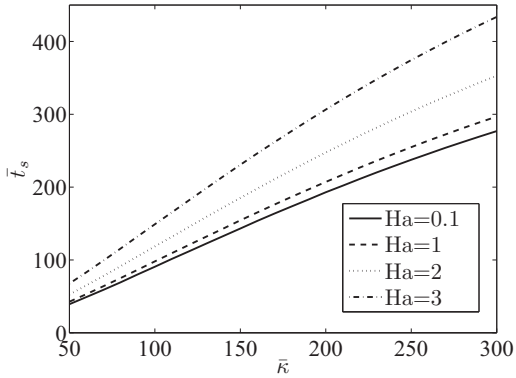

FIG. 6. Stopping time ($\bar{t}_s$) vs $\bar{\kappa}$ for varying Ha = 0.1, 1, 2, and 2.5, with $\theta = 20°$ and $\zeta_0 = 50$ mV.

good agreement is observed between the scaling estimates and the numerically plotted times. As mentioned in the previous section, the filling time remains constant for low values of Hartmann numbers and increases approximately proportionally to the square of Ha for higher values of the same. This same feature is qualitatively verified in Fig. 4(a), where the delay in the time for the capillary to stop is obvious. This increase in the stopping time ($\bar{t}_s$) indicates that the capillary motion is sustained for greater extent of time, although the equilibrium length remains the same.

Figure 6 depicts the variation in stopping time ($\bar{t}_s$) with $\bar{\kappa}$ for various values of Ha. It can be observed that the filling time gets augmented when the Debye layer goes thinner, as attributable to increased viscous resistance to the flow along with an increased opposing electrical body force.

In essence, we can state that in cases of positive zeta potential on the walls, the capillary mimics its motion under the action of gravity and surface tension, as the capillary stops rising after traversing a certain distance, when its motion is opposed by the external electric field. However, this equilibrium distance can be intricately controlled, by tuning various parameters, such as the electric field strength, the Debye length, and the zeta potential, along with the geometric parameters. The general trend is that, whenever the capillary slows down, the equilibrium length $\bar{L}_s$ decreases, whereas the time taken by the capillary to reach the equilibrium position is increased. This slowing down might stem from different sources, such as an increase in total drag resistance for increased Ha or $\bar{\kappa}$, or a drop in the forward pulling force due to increased contact angle at the interface. It has been demonstrated that, even if the equilibrium length drops, which will make the capillary traverse less distance, the time taken always increases for an even larger decrease in the velocity of the capillary front.

2. Implications of negative zeta potential

Unlike positive zeta potentials, negative zeta potential on the walls actually aids the capillary motion as evident from Eqs. (8) and (21). Therefore, the fluid does not stop in such cases and essentially witnesses perpetual advancement along the channel. The liquid front eventually crosses the far side electrode positioned at $\bar{x} = 1$ and experiences a constant electrical body force from then onwards, as depicted in the previous section.

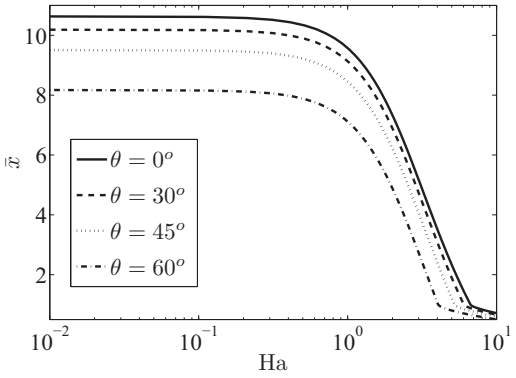

FIG. 7. $\bar{x}$ (distance traversed by the liquid front after time $\bar{t} = 100$) vs Ha for varying $\theta = 0°, 30°, 45°$, and $60°$, with $\zeta = -50$ mV and $\bar{\kappa} = 100$.

Figure 7 demonstrates the variation in the distance reached by the capillary ($\bar{x}$) after time $\bar{t} = 100$, with Ha, for different values of the contact angles. We observe a decline in the values of distance traversed with a corresponding increase in Ha, which stems from an increased resistance to the flow for an increase in the magnetic field strength. A sudden change in the length traversed is observed around $\bar{x} = 1$, as electrical body force becomes constant from then onwards. For relatively higher Ha, the liquid front is not able to cross the far side electrode, for the time considered in the present figure.

C. Possibility of existence of oscillatory regime

Previously, researchers have demonstrated [6–9,31] that for capillary filling with low viscosity fluids, the Washburn regime can be potentially replaced by an oscillatory regime, where the capillary front undergoes damped oscillations around the "Jurin" height and eventually stops. In these cases, the linear regimes are directly followed by the oscillatory regime, since the viscous forces are low. Here we also attempt to investigate the possibility of occurrence of a similar oscillatory regime by tuning various relevant parameters, most notably the magnitude of the actuating electric field. Following Das and Mitra [9], we note that the governing Eq. (21) can be expressed in the following equivalent form:

$$\frac{d}{d\bar{t}}\left[\left(\bar{x} + \frac{\pi H}{8L}\right)\frac{d\bar{x}}{d\bar{t}}\right] = A - B\frac{\bar{x}}{\bar{x} + (1-\bar{x})\bar{\varepsilon}} - C\bar{x}\frac{d\bar{x}}{d\bar{t}}. \tag{32}$$

In Eq. (32), $A = \cos\theta$, $B = \frac{(E_0 L)\varepsilon_l \zeta \bar{\kappa}\tanh(\bar{\kappa}/2)}{\sigma H}$, and $C = \frac{L}{\sqrt{2\sigma\rho H}}\left(\frac{\mu \mathrm{Ha}^2}{H} + \eta\right)$. It was demonstrated by Das and Mitra [9] that for a choice of $C/B \sim 0.1$–0.01, the capillary front underwent oscillations about the "Jurin" height. Considering the above range, we plot the positions ($\bar{x}$) of the capillary front with time for $A = 1$ and for the following three values of the C/B ratios: 0.001 68, 0.003 36, and 0.0168, as shown in Fig. 8. Quite intuitively, a small C/B ratio indicates that the viscous forces are quite small as compared to the electrical body forces acting on the liquid front. We observe from the present figure that for $C/B \ll 1$, the capillary front undergoes clear oscillations about the equilibrium height. As we increase the value of this ratio, oscillations slowly tend to die down and

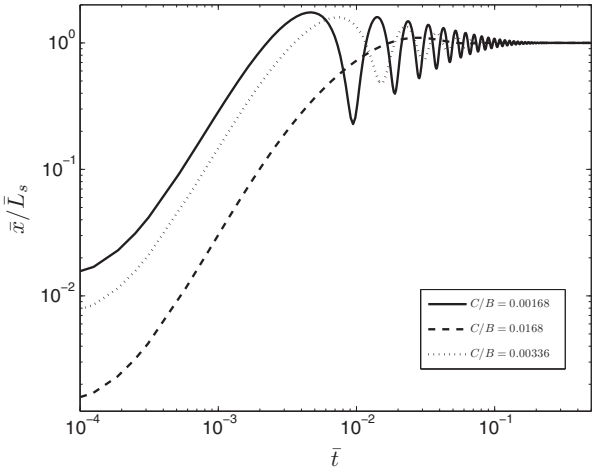

FIG. 8. Solution of Eq. (32) with $A = 1$ and different C/B ratios, as stated in the inset. We note that for $C/B = 0.001\,68$ we observe oscillations of the capillary front, whereas for higher values of the same this oscillation is not so prominent. However, such small ratios for C/B are not practically possible to achieve for the given setup.

for values of C/B close to 1, the oscillations cease to exist and the capillary front directly reaches the equilibrium height.

Previously Das and Mitra [9] demonstrated that the condition for the existence of the oscillatory regime is dictated by the ratio of the Ohnesorge (Oh) number to the Bond number (Bo), which typifies the ratios of the viscous force and gravity. In the present analysis, gravity is basically replaced by the electrical body force. Therefore, we first attempt to determine the orders of magnitudes of the viscous and the electrical forces. Towards this we note that, in Sec. III A 2, we have already shown that the viscous drag (per unit width) scales as $F_{\mathrm{visc}} \sim \mu u \kappa x$. The electrical body force simply scales as $F_{\mathrm{elec}} \sim q E_{\mathrm{ref}}$, where q is the total charge, which, per unit width, which in turn is on the order of $q \sim \varepsilon_l \zeta \kappa x$, thus making $F_{\mathrm{elec}} \sim \varepsilon_l \zeta \kappa x E_{\mathrm{ref}}$. The ratio of the two forces is then $\frac{F_{\mathrm{visc}}}{F_{\mathrm{elec}}} \sim \frac{\mu u}{\varepsilon_l \zeta E}$. Now, we recall from the Eq. (22b) that $u \sim x/t \sim \sqrt{\sigma/\rho H}$, which makes the ratio $\frac{F_{\mathrm{visc}}}{F_{\mathrm{elec}}} \sim \mathrm{Oh}(\frac{\sigma}{\varepsilon_l E \zeta})$. Hence it follows that the condition $\mathrm{Oh}/\beta \ll 1$ $[\beta^{-1} = \sigma/(\varepsilon_l E \zeta)]$ is equivalent to $\mathrm{Oh}/\mathrm{Bo} \ll 1$, which will lead to the existence of an oscillatory solution. In the same spirit, for $\mathrm{Oh}/\beta \sim 1$ or $\mathrm{Oh}/\beta \gg 1$, the capillary front will witness significant viscous forces which will finally lead to preclusion of the oscillatory regime. We note from Fig. 8 that Oh/β turns out to be 0.0011 for $C/B = 0.001\,68$, which is much smaller than unity. However, in the earlier figures, for example, in Fig. 4(a), the C/B ratio is $C/B = 16.82 \gg 1$ (for $C = 163.71$ and $B = 9.73$), which makes $\mathrm{Oh}/\beta = 10.7573$ and hence no oscillations are observed.

We now investigate the probable values of the applied electric fields and related parameters for which we can obtain the oscillatory regime in capillary filling dynamics. As mentioned earlier, usually for water $\mathrm{Oh} \sim 0.005$ for channel height on the order of $\sim 10^{-4}$ m. Noting that $\varepsilon_l \sim 6 \times 10^{-10}$, $\zeta \sim 50$ mV, it follows that for $\mathrm{Oh}/\beta \ll 1$ to be satisfied, $E \gg 10^7$ V/m. In fact, in Fig. 8, for $C/B = 0.001\,68$, we get $E \sim 10^{10}$ V/m, taking water as the filling liquid. Noting that the breakdown potential for water is about 7×10^7 V/m, it becomes obvious that taking water as the filling liquid, it is practically impossible

to obtain the oscillatory regime. Even for very low viscosity organic fluids, the field strength needs to be very high in order to obtain the oscillatory regime. Therefore it can be inferred from the present analysis that for electrically actuated capillary motion the oscillatory regime is extremely difficult and probably practically impossible to obtain, in contrast to gravity-influenced capillary filling, where the presence of an oscillatory regime has been experimentally verified [6,7].

V. COMPARISON WITH EXPERIMENTS

In this section we take a brief look at the available experimental techniques for capillary motion and also compare our results with the previously reported pertinent experimental work.

A. A brief review of available experimental techniques for capillary filling and Electro-Magneto-Hydrodynamics

Experiments on capillary filling are abundant in the literature, where the filling process has been observed for a number of different fluids. Lucas [3] was among one of the earliest to perform experiments on capillary filling for a series of different fluids. Around the same time, Washburn also performed experiments on capillary filling [4], in vertical channels. Both Lucas [3] and Washburn [4] provided theoretical models for the filling process, which match with the experimental predictions to a great extent. A detailed review of a standard capillary filling experimental setup can be found in the seminal work of Washburn [4].

In more recent years, Quere [7] has done experiments in vertical capillary filling, for a number of organic and inorganic fluids. His experimental results revealed oscillation of a capillary front near the Jurin or equilibrium height, for fluids with low viscosities. Very recently, these oscillations have also been obtained from theoretical considerations by Zhmud *et al.* [6] and Das and Mitra [9]. Experiments of Quere [7] have also revealed the existence of a linear x vs t regime of filling, preceding the much celebrated Washburn regime, where the $x \sim \sqrt{t}$ relation for filling is followed. Existence of such regime has also been predicted by theoretical [8,9] as well as molecular dynamics simulations [25] in recent years. In our analysis we have depicted that in the present case also, there exists a linear regime; i.e., the $x \sim t$ relation is witnessed for the initial times of capillary filling. More recently, Radiom *et al.* [32] have performed experiments on filling in closed capillaries with entrapped gas and have shown that the capillary comes to an equilibrium position as it is pressurized by the entrapped gas. Additionally, Ichikawa *et al.* [33] have performed experiments on capillary filling in rectangular microchannels, along with theoretical predictions through numerical simulations of capillary motion equations. Barraza *et al.* [34] have performed experiments on advancing contact lines of Newtonian fluids, between two parallel plates.

A close review of these and many more studies on capillary filling suggests that the experimental setup for studying capillary filling process is a fairly standard one, the details of which can be found in any of the papers referenced above. Since our work also involves electrokinetic and magnetic actuation of liquid, it is desirable to include a brief review of the previously reported experimental studies on electro-osmosis and magneto-hydrodynamics. Experiments on electro-osmotic flows (EOF) are aplenty in the literature [35–39], dealing with steady EOFs with uniform surface potential [36] and EOFs with patterned surface potential [37], which generate recirculation rolls in fluids. In more recent times, a number of experimental studies on ac electro-osmosis have been performed [35,38,39], where asymmetric arrays of electrodes on the surfaces with ac potential generate net finely tunable flows. Experiments on magneto-hydrodynamics have also been performed, a number of which are focused towards designing of magneto-hydrodynamic (MHD) pumps [40–42]. Previously, Huang *et al.* [41] have devised a microfluidic magneto-hydrodynamic pumping apparatus using conventional machining techniques; a slightly different MHD micropump was designed and tested by Jang and Lee [42], where the directions of the fields were changed. A detailed review of the setup used for the experiments can, again, be found in the aforementioned papers. However, experimental studies on capillary filling with electrical and magnetic effects are relatively scarce. In recent years, Phan *et al.* [27] have performed experiments on capillary filling in open-end and closed-end nanochannels with electrolyte solutions, where the walls of the capillary had induced charge or potential. In the next subsection, we will attempt to match our solutions with the experimental results of Phan *et al.* [27].

B. Comparison of present theory with experiments

As mentioned earlier, in this subsection we are going to compare the results from our present analysis with the experimental results previously reported by Phan *et al.* [27]. Their setup consisted of different lengths of nanochannels (500 μm, 1 mm, 1.5 mm, 2 mm, and 2.5 mm), while the channels were of two different heights $H = 45$ nm and 80 nm, the width of the channel being constant at $w = 10\,\mu$m. Among all the results reported by Phan *et al.*, we here (for the sake of brevity) chose to compare our results for filling of ethanol into a horizontal closed capillary in the 45-nm channel (Fig. 7(a) in Ref. [27]). Towards this, we first solve the corresponding governing equations for capillary filling and then proceed towards matching the solutions with the experimental data. In this case, as explained by Phan *et al.* [27], the electric field will be an induced one, instead of being externally applied. In other words, the electric field acting upon the fluid in the present case is nothing but the streaming electric field. The basic equation here for capillary filling remains Eq. (18), with an additional forcing term that comes in because of the presence of entrapped air [27,32]. Including this force, the equation for capillary filling becomes [27,32]

$$\frac{d}{dt}\left[\left(\rho H x + \frac{\rho \pi H^2}{8}\right)\frac{dx}{dt}\right] = 2\sigma\cos\theta - F_e - Vx\frac{dx}{dt} - \frac{p_0 H x}{L_0 - x}. \tag{33}$$

The last term in (33) is the contribution of the entrapped air in the channel [27,32], assuming that the gas follows Boyle's law. Here, F_e is the body force generated from the streaming potential, given by $F_e = \int_0^x E_s ds \int_{-H/2}^{H/2} \rho_e(y) dy$, where E_s is

the streaming electric field. In Eq. (33), V is given by $V = \frac{2\mu}{H}\frac{(\bar{F}_1+G\bar{F}_2)}{(K_1+GK_2)}$, while the rest of the symbols have already been mentioned in the discussion following Eq. (15). From this form of the viscous force we can appreciate the advantage gained by the general formulation of the viscous forces that was done previously (please refer to Sec. II). Here, we must take the pressure gradient into account, since the streaming electric field is directly proportional to the pressure gradient and hence the term F_1 (which bears the effect of the pressure gradient) cannot be neglected. The constants are given by

$$\bar{F}_1 = \lim_{\mathrm{Ha}\to 0} \tanh(\mathrm{Ha}/2)/\mathrm{Ha} = 1/2,$$

$$\bar{F}_2 = -\lim_{\mathrm{Ha}\to 0} \frac{\bar{\kappa}^2}{\bar{\kappa}^2 - \mathrm{Ha}^2}\{\mathrm{Ha}\tanh(\mathrm{Ha}/2) - \bar{\kappa}\tanh(\bar{\kappa}/2)\} = \bar{\kappa}\tanh\left(\frac{\bar{\kappa}}{2}\right),$$

$$K_1 = \lim_{\mathrm{Ha}\to 0} \frac{1}{\mathrm{Ha}^2}\left\{1 - \frac{\tanh(\mathrm{Ha}/2)}{(\mathrm{Ha}/2)}\right\} = \frac{1}{12},$$

and

$$\mathrm{K}_2 = -\lim_{\mathrm{Ha}\to 0} \frac{\bar{\kappa}^2}{\bar{\kappa}^2 - \mathrm{Ha}^2}\left\{\frac{\tanh(\bar{\kappa}/2)}{(\bar{\kappa}/2)} - \frac{\tanh(\mathrm{Ha}/2)}{(\mathrm{Ha}/2)}\right\} = 1 - \frac{\tanh(\bar{\kappa}/2)}{\bar{\kappa}/2}.$$

Now, to specify G, we need to calculate the streaming potential. This is done by making the total current, i.e., the sum of streaming and conduction current zero [43]. This can be expressed in the following form:

$$\int_{-H/2}^{H/2} \rho_e u_p dy + \int_{-H/2}^{H/2} \rho_e u_e dy + \sigma_e E_s H = 0. \tag{34}$$

In (34) E_s is the streaming electric field, and $u_p(y) = -\frac{1}{2\mu}\frac{dp}{dx}(\frac{H^2}{4} - y^2)$ and $u_e(y) = -\frac{\varepsilon_l E_s \zeta}{\mu}[1 - \frac{\cosh(\kappa y)}{\cosh(\kappa H/2)}]$, while the charge density is given by Eq. (4). Equivalently, one can write

$$\Rightarrow \frac{dp}{dx} I_p + E_s I_e + \sigma_e E_s H = 0, \quad \text{or} \quad \frac{E_s}{dp/dx} = -\frac{I_p}{I_e + \sigma_e H} = G_1. \tag{35}$$

In (35), the I_p and I_e are given by

$$I_e = \frac{C_1(\bar{\kappa} + \sinh(\bar{\kappa}))}{2\kappa\cosh(\bar{\kappa}/2)} - \frac{2C_1}{\cosh(\mathrm{Ha}/2)}\left[\frac{(\mathrm{Ha}/H)\sinh(\mathrm{Ha}/2)\cosh(\bar{\kappa}/2) - \kappa\cosh(\mathrm{Ha}/2)\sinh(\bar{\kappa}/2)}{(\mathrm{Ha}/H)^2 - \kappa^2}\right],$$

$$C_1 = -\frac{\varepsilon_l^2\zeta^2 H^2\kappa^4}{\eta\cosh(\bar{\kappa}/2)(\bar{\kappa}^2 - \mathrm{Ha}^2)},$$

$$I_p = \frac{2C_2\sinh(\bar{\kappa}/2)}{\kappa} - \frac{2C_2}{\cosh(\mathrm{Ha}/2)}\left[\frac{(\mathrm{Ha}/H)\sinh(\mathrm{Ha}/2)\cosh(\bar{\kappa}/2) - \kappa\cosh(\mathrm{Ha}/2)\sinh(\bar{\kappa}/2)}{(\mathrm{Ha}/H)^2 - \kappa^2}\right],$$

$$C_2 = -\frac{\varepsilon_l\zeta\kappa^2 H^2}{\eta\mathrm{Ha}^2\cosh(\bar{\kappa}/2)}.$$

The electrical body force is then given by

$$F_e = \int_0^x E_s ds \int_{-H/2}^{H/2} \rho_e(y) dy = -2xG_1\frac{dp}{dx}\kappa\varepsilon_l\zeta\tanh(\bar{\kappa}/2). \tag{36}$$

We further note that the average velocity in the present case can be expressed as

$$\frac{dx}{dt} = -\frac{H^2}{\eta}\frac{dp}{dx}(K_1 + GK_2). \tag{37}$$

Therefore, in conjunction with (37), the electrical body force in (36) can be expressed as

$$F_e = \frac{G_1 Q}{(-H^2/\eta)(K_1 + GK_2)} x\frac{dx}{dt}, \quad \text{where}$$

$$G = -\frac{\varepsilon_l\zeta}{H^2}G_1 \quad \text{and} \quad Q = -2\kappa\varepsilon_l\zeta\tanh(\bar{\kappa}/2). \tag{38}$$

Combining all the forces, as derived earlier, the final equation for the motion of the liquid front can be written as

$$\frac{d}{dt}\left[\left(\rho Hx + \frac{\rho\pi H^2}{8}\right)\frac{dx}{dt}\right] = 2\sigma\cos\theta - (E+V)x\frac{dx}{dt} - \frac{p_0 Hx}{L_0 - x},$$

$$E = \frac{G_1 Q}{(H^2/\eta)(K_1 + GK_2)}. \tag{39}$$

Since the channel dimension is small, the effect of inertia can be safely neglected [4,27], based on the fact that the liquid mass in the capillary will be very small. Therefore, we recast

Eq. (39) in the following form, neglecting the inertial effects:

$$\frac{dx}{dt} = \frac{N_1 A}{x} - \frac{N_2 B}{L_0 - x}, \text{ where}$$
$$A = \frac{2\sigma\cos\theta}{\beta_1}, \quad B = \frac{p_0 H}{\beta_1}, \text{ and } \beta_1 = E + V. \quad (40)$$

In Eq. (40) we have multiplied the forward pulling capillary force and the resistive forces with prefactors N_1 and N_2, respectively. The significance of these prefactors is discussed subsequently. The solution to Eq. (40) can easily be obtained in the form $t = f(x)$ with the initial condition $x(t = 0) = 0$ in the following form:

$$t = -\frac{N_1 N_2 A B L_0^2}{(N_1 A + N_2 B)^3} \log\left(1 - \frac{N_1 A x + N_2 B x}{N_1 A L}\right) - \frac{N_2 B L x}{(N_1 A + N_2 B)^2} + \frac{x^2}{2(N_1 A + N_2 B)}. \quad (41)$$

From (41), one can easily compute the position of the capillary front (x) as a function of time through any numerical method (for example, the Newton-Raphson method). Note that with $N_1 = N_2 = 1$, the form of the solution is identical to that obtained by Phan *et al.* [27]. Figure 9 shows the experimental data of Phan *et al.* [27], along with the theoretical predictions based on Eq. (41), for capillary filling of ethanol. The other relevant parameters have been mentioned in the caption of the figure. It can be noted from the figure that good agreement between the theory and experiment is observed for all the reported cases, i.e., channel lengths. It is important to mention here that the relevant liquid properties along with the Laplace pressure have been taken from the paper of Phan *et al.* [27] and the zeta potential (ζ) has been taken to be 25 mV.

Finally, it is important to mention the significance of the factors N_1 and N_2. Similar prefactors have previously been used by Phan *et al.* (through augmentation of apparent viscosity [27]) and Das and Mitra [9] for comparison with experimental data. A detailed discussion on these factors can thus be found in the later work [9]. However, for the sake of completeness, we briefly mention here the physical significance of these constants. The factor N_1 basically alters the forward pulling capillary force. Therefore, this constant signifies the effect of dynamically evolving contact angle [9,12,32]. Additionally, we have used a parallel plate geometry for the present theoretical predictions, although in the experiments rectangular channels were used. Therefore, the resulting capillary force will be larger in case four walls are bounding the surface instead of two walls. Hence N_1 can be considered as a combination of all these factors, augmenting the capillary force in the process. On the other hand, N_2 primarily signifies augmented viscous and resistive forces. It is based on the fact that typical capillary filling is characterized by three regimes [12,44], entry, Poiseuille, and meniscus traction regime. We have mainly considered the second regime, i.e., the Poiseuille regime, for our study and accordingly have calculated the drag as shown in Eq. (15). However, the other two regimes, specifically the meniscus traction regime, offers greater viscous drag to the advancing liquid front and therefore the net viscous drag increases. Apart from this, the viscous drag is also somewhat augmented due to the presence of sidewalls, in a rectangular microchannel, used in the experiments. Therefore, the constant N_2 is a combination of all these factors, which results in higher viscous drag.

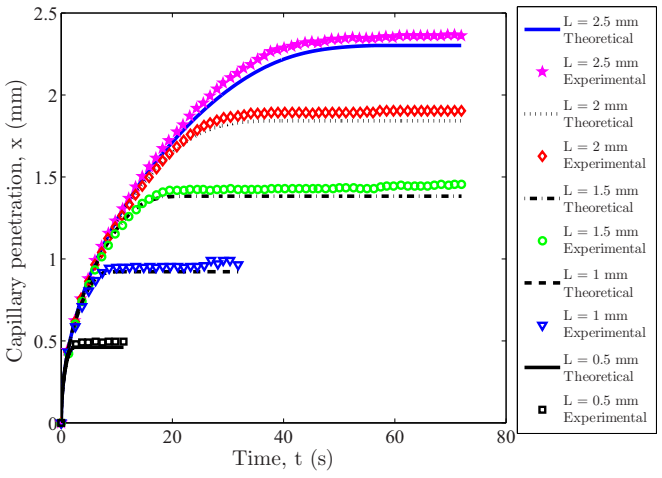

FIG. 9. (Color online) Plot showing comparison of experimental results with the theoretical model for capillary filling of ethanol under streaming potential field. The fluid property values are $\varepsilon_l = 2.16 \times 10^{-10}$ F/m, $\mu = 1.0036 \times 10^{-3}$ Pa s, $\rho = 789$ kg/m^3, $\sigma = 0.0224$ N/m, Laplace pressure $= 9.96 \times 10^5$ N/m^2. Other simulation parameters are N_2 (viscous drag factor) $= 2.5$ and N_1 (Laplace pressure factor) $= 1.2$. The zeta potential is $\zeta = 25$ mV and $\kappa H = 26.6$.

VI. CONCLUSIONS

In the present study, we have assessed the capillary filling dynamics in microfluidic channels in the presence of electromagneto-hydrodynamic interactions, simultaneously subjected to EDL effects. We have considered an axial electric field and transverse magnetic field acting on an electrolyte in a parallel plate channel configuration. We have delineated the consequences of magneto-viscous effects on various regimes of the capillary filling dynamics. We have demonstrated that for positive zeta potential on the channel walls, the liquid front can mimic its motion under the action of equivalent gravitational force. We have executed a scaling analysis of the relevant forces and have also derived a long term solution for the cases of positive zeta potential. Our scaling estimates reveal that the initial linear regime in the capillary filling also exists in the present case, but for a very short duration of time, since the viscous forces start dominating within a very short distance of capillary imbibition. The present scaling analysis along with the semianalytical approach also reveals the occurrence of a modified Washburn regime.

We have further investigated the time taken by the capillary to reach the equilibrium height for different combinations of parameters, and have shown that the filling time increases with corresponding increase in the values of Hartmann number and inverse of the characteristic EDL thickness. We have additionally executed a scaling analysis to estimate the capillary filling time as a function of the Hartmann number and worked out two different regimes of variations in the filling time with the same. Our analysis also points out that the previously reported oscillatory capillary filling regime can be obtained

only under extreme conditions, which become impossible to realize in experimental practice. In the penultimate section we have presented a review of some of the previous experiments performed on capillary filling, under various conditions. We have also compared our results to a relevant experiment in capillary filling and found good agreement between theoretical prediction and experimental data.

The practical significance of the present study can be far reaching. Following the inferences drawn from the present study, it can be concluded that interplay between the induced electric field due to EDL effects and the externally applied electrical and magnetic fields may alter the classical notion of capillary filling dynamics in a rather interesting and scientifically intriguing manner. From a more application oriented perspective, the external electric and magnetic fields can be judiciously employed as tuning parameters towards modulating the dynamics of capillary filling in a rather intricate manner, bearing immense consequences towards designing on-chip micro–total analysis systems for medical diagnostics and other important applications.

[1] H. A. Stone, A. D. Stroock, and A. Ajdari, Annu. Rev. Fluid. Mech. **36**, 381 (2004).

[2] R. B. Schoch, J. Han, and P. Renaud, Rev. Mod. Phys. **80**, 839 (2008).

[3] R. Lucas, Kolloid-Z. **23**, 15 (1918).

[4] E. W. Washburn, Phys. Rev. **17**, 273 (1921).

[5] C. H. Bosanquet, Philos. Mag. **45**, 525 (1923).

[6] B. V. Zhmud, F. Tiberg, and K. Hallstensson, J. Colloid Interface Sci. **228**, 263 (2000).

[7] D. Quere, Europhys. Lett. **39**, 533 (1997).

[8] S. Das, P. R. Waghmare, and S. K. Mitra, Phys. Rev. E **86**, 067301 (2012).

[9] S. Das and S. K. Mitra, Phys. Rev. E **87**, 063005 (2013).

[10] S. Chakraborty and D. Paul, J. Phys. D: Appl. Phys. **39**, 5364 (2006); S. Chakraborty, Z. Duan, and Y. S. Muzychka, Phys. Fluids **20**, 043602 (2008).

[11] C. P. Tso and K. Sundaravadivelu, J. Phys. D: Appl. Phys. **34**, 3522 (2001).

[12] S. Chakraborty, Anal. Chim. Acta **605**, 175 (2007); Lab Chip **5**, 421 (2005).

[13] S. Das and S. Chakraborty, Anal. Chim. Acta **559**, 15 (2006).

[14] J. Yang, F. Lu, and D. Y. Kwok, J. Chem. Phys. **121**, 7443 (2004).

[15] J. A. Thomas, M. P. Boyle, L. W. Hunter, and J. E. Tiffany, J. Colloid Interface Sci. **372**, 176 (2012).

[16] N. R. Tas, J. Haneveld, H. V. Jansen, M. Elwenspoek, and A. van den Berg, Appl. Phys. Lett. **85**, 3274 (2004).

[17] A. Han, G. Mondin, N. G. Hegelbach, N. F. de Rooij, and U. Staufer, J. Colloid Interface Sci. **293**, 151 (2006).

[18] J. W. van Honschoten, J. W. Berenschot, T. Ondarçuhu, R. G. P. Sanders, J. Sundaram, M. Elwenspoek, and N. R. Tas, Appl. Phys. Lett. **97**, 014103 (2010).

[19] J. M. Oh, T. Faez, S. de Beer, and F. Mugele, Microfluid. Nanofluid. **9**, 123 (2010).

[20] P. Waghmare and S. K. Mitra, Microfluid. Nanofluid. **12**, 53 (2012); Anal. Chim. Acta **663**, 117 (2010); A. Saha and S. K. Mitra, J. Colloid Interface Sci. **339**, 461 (2009); A. Saha, S. K. Mitra, M. Tweedie, S. Roy, and J. McLaughlin, Microfluid. Nanofluid. **7**, 451 (2009).

[21] A. Kutana and K. P. Giapis, Nano Lett. **6**, 656 (2006).

[22] D. I. Dimitrov, A. Milchev, and K. Binder, Phys. Rev. Lett. **99**, 054501 (2007).

[23] N. Ichikawa and Y. Satoda, J. Colloid Interface Sci. **162**, 350 (1994).

[24] M. Dreyer, A. Delgado, and H. Rath, J. Colloid Interface Sci. **163**, 158 (1994).

[25] L. Joly, J. Chem. Phys. **135**, 214705 (2011).

[26] S. Supple and N. Quirke, Phys. Rev. Lett. **90**, 214501 (2003).

[27] V. N. Phan, P. Joseph, L. Djeghlaf, A. E. D. Allouch, D. Bourrier, P. Abgrall, A.-M. Gue, C. Yang, and N-T. Nguyen, Heat Transfer Eng. **32**, 1 (2011).

[28] J. Israelachvili, *Intermolecular and Surface Forces* (Academic Press, London, 1992).

[29] J. Chakraborty and S. Chakraborty, in *Mechanics Over Micro and Nano Scales*, edited by S. Chakraborty (Springer, New York, 2011), pp. 1–60.

[30] L. G. Leal, *Advanced Transport Phenomena: Fluid Mechanics and Convective Transport Processes* (Cambridge University Press, Cambridge, 2007).

[31] G. Ramon and A. Oronb, J. Colloid Interface Sci. **327**, 145 (2008).

[32] M. Radiom, W. K. Chang, and C. Yang, Microfluid. Nanofluid. **9**, 65 (2010).

[33] N. Ichikawa, K. Hosokawa, and R. Maeda, J. Colloid Interface Sci. **280**, 155 (2004).

[34] H. J. Barraza, S. Kunapuli, and E. A. O'Rear, J. Phys. Chem. B **106**, 4979 (2002).

[35] V. M. Barragan and C. R. Bauza, J. Colloid Interface Sci. **230**, 359 (2000).

[36] F. H. J. van der Heyden, D. J. Bonthuis, D. Stein, C. Meyer, and C. Dekker, Nano. Lett. **6**, 2232 (2006).

[37] A. D. Stroock, M. Weck, D. T. Chiu, W. T. S. Huck, P. J. A. Kenis, R. F. Ismagilov, and G. M. Whitesides, Phys. Rev. Lett. **84**, 3314 (2000).

[38] A. B. D. Brown, C. G. Smith, and A. R. Rennie, Phys. Rev. E **63**, 016305 (2000).

[39] N. G. Green, A. Ramos, A. Gonzalez, H. Morgan, and A. Castellanos, Phys. Rev. E **61**, 4011 (2000).

[40] S. Ghosh, C. Yang, T. Cai, Z. Hu, and A. Neogi, J. Phys. D **42**, 135501 (2009).

[41] L. Huang, W. Wang, M. C. Murphy, K. Lian, and Z. G. Ling, Microsyst. Technol. **6**, 235 (2000).

[42] J. Jang and S. S. Lee, Sens. Actuators, B **80**, 84 (2000).

[43] M.-S. Chun, T. S. Lee, and N.-W. Choi, J. Micromech. Microeng. **15**, 710 (2005).

[44] W. Huang, R. S. Bhullar, and Y. C. Fung, J. Biomech. Eng., **123**, 446 (2001).